Heliyon 9 (2023) e17977

Contents lists available at ScienceDirect

Heliyon

journal homepage: www.cell.com/heliyon

# Construction novel polybenzoxazine coatings exhibiting corrosion protection of mild steel at different concentrations in a seawater solution

Abdulsalam Mahdy [a,b,*], Kamal I. Aly [a], Mohamed Gamal Mohamed [a,**]

[a] Polymer Research Laboratory, Chemistry Department, Faculty of Science, Assiut University, Assiut 71516, Egypt
[b] Chemistry Department, Faculty of Education & Science, Rada'a Albaydha University, Al-Baydha 38018, Yemen

ARTICLE INFO

*Keywords:*
Schiff base moiety
Benzoxazine
Ring-opening polymerization
Polybenzoxazine
Electrochemical measurements
Anticorrosion efficacy

ABSTRACT

In this work, a new and effective polymeric coating is used to improve mild steel's corrosion resistance. The coating incorporates a Schiff base moiety into a benzoxazine (BZ) precursor, resulting in improved protection against corrosion. The SF-Tol-BZ polymerization behavior and thermal properties were studied using differential scanning calorimetry (DSC) and thermal-gravimetric analysis (TGA), respectively, at different curing temperatures. The poly(SF-Tol-BZ) cured at 240 °C had a $T_{d10}$ value of 604 °C and a Tg of 225 °C. The efficacy of poly(SF-Tol-BZ) coatings in protecting mild steel (MS) from corrosion in a NaCl (3.5%) solution at room temperature was evaluated using various corrosion measurements, including open circuit potential (OCP), and electrochemical impedance spectroscopy (EIS). The results showed that increasing the poly(SF-Tol-BZ) concentration led to a corresponding increase in its protective efficiency, reaching a maximum of 92% at a concentration of 300 g/L. The coatings also exhibited a 24-fold increase in Rct values and a one-order-of-magnitude reduction in CPE compared to the bare mild steel. Finally, the poly(SF-Tol-BZ) precursors demonstrated a $CO_2$ uptake of 23 mg $g^{-1}$ (measured at 298 K).

## 1. Introduction

Corrosion is a natural process where materials, especially metals, can be destroyed through chemical and electrochemical reactions with their surroundings. Corrosion is thought to cost the world economy over US$2.5 trillion per year [1]. Metals, particularly carbon steel, are widely used in the industrial field due to their good mechanical properties, low cost, excellent, and availability [2]. However, due to their remarkable anti-corrosion properties and eco-friendliness, conducting polymers have gained more and more attention as protective coatings or as film-forming corrosion inhibitors [3]. Organic coatings frequently prevent corrosion on metal surfaces by creating a barrier layer. Due to their high electron density from heteroatoms like oxygen, nitrogen, sulfur, and aromatic rings, they have been demonstrated to be efficient anti-corrosion inhibitors for mild steel in a variety of corrosive conditions [4–9]. Due to its low dielectric constants, low water absorption, and good chemical and heat resistance, polybenzoxazine (PBZ) is a promising material for corrosion prevention [10–15]. Schiff bases materials have also been reported to be effective corrosion inhibitors for metals like mild

* Corresponding author. Polymer Research Laboratory, Chemistry Department, Faculty of Science, Assiut University, Assiut 71516, Egypt.
** Corresponding author.
*E-mail addresses:* abdualsalamaljbri@baydaauniv.net (A. Mahdy), mgamal.eldin12@aun.edu.eg (M.G. Mohamed).

https://doi.org/10.1016/j.heliyon.2023.e17977
Received 27 March 2023; Received in revised form 3 July 2023; Accepted 4 July 2023
Available online 6 July 2023

steel, aluminum, zinc, and copper in corrosive media. This is because they tend to absorb onto a metal surface, thereby hindering active corrosion centers [16–20]. Moreover, it has been found that Schiff bases with aromatic rings and –C=N- groups in their molecular structure are better corrosion inhibitors than their corresponding amines and aldehydes [21,22]. Chitosan salicylaldehyde Schiff base has also been shown to inhibit corrosion on Q235 steel through adsorption onto its surface [23]. Another study reported that chitosan vanillin material inhibited the corrosion process on mild steel (MS) by forming a protective layer on its surface, which was confirmed using AFM and WCAs analyses [24]. In addition, polybenzoxazine has been used in various applications, including antifouling and anticorrosion coatings [25,26], high flame retardancy polymers [27], high voltage insulation materials [28], and is a perfect candidate for deriving carbon structures with applications catalysis, beyond energy, and environment. Using it in carbon materials is due to its high char yield following carbonization [29]. Currently, two approaches suggested to soften polybenzoxazine coatings are introducing nanofiller (e.g., carbon nanotube) [30] or plastic polymers to alloy polybenzoxazine [31], the other is introducing flexible silane or alkyl long-chain segments to the branched-chain or backbone of benzoxazine monomers [32,33]. This study focuses on introducing an effective Schiff base moiety into a benzoxazine precursor through molecular design. The aim is to enhance the corrosion protection of MS by developing polybenzoxazine (e.g., poly(SF-Tol-BZ)) coatings. The effectiveness of these coatings in a seawater environment was evaluated using various techniques, including open circuit potential (OCP), potentiodynamic polarization (Tafel curves), and electrochemical impedance spectroscopy (Nyquist and Bode plots). Additionally, the corrosion protection mechanism was elucidated. The polymerization behavior and thermal stability of the SF-Tol-BZ monomer and its corresponding PBZ were investigated through thermogravimetric analysis (TGA), differential scanning calorimetry (DSC), and Fourier-transform infrared spectroscopy (FTIR) analyses at different curing temperatures. Furthermore, the $CO_2$ uptake of poly(SF-Tol-BZ) after curing temperature at 240 °C was evaluated through BET measurement.

## 2. Experimental

### 2.1. Material

1,4-Phenylenediamine ($C_6H_8N_2$, 97%), terephthalaldehyde, 4-hydroxybenzaldehyde ($C_7H_6O_2$, 98%), paraformaldehyde (97%), *p*-toluidine (≥99.5%), chloroform, methanol, toluene, ethanol, and acetone were obtained from different commercial suppliers. The starting material (SF-BZ 2OH) was prepared as previously reported [34,35] (as depicted in Scheme 1).

### 2.2. Preparation of Schiff base functional BZ monomer (SF-Tol-BZ) [35]

To prepare SF-Tol-BZ, SF-BZ 2OH, *p*-toluidine, and paraformaldehyde were reacted together in the presence of toluene/ethanol (2:1). Specifically, 6.33 mmol (2 g) of SF-BZ 2OH, 13.1 mmol (1.4 g) of *p*-toluidine, and 26.7 mmol (0.8 g) of paraformaldehyde were mixed and stirred at 80 °C for 3 h. The resulting solid residue was then dissolved in chloroform (50 mL) and washed with 0.5 N sodium carbonate solutions before being dried over a layer of magnesium sulfate. Upon evaporating the chloroform, SF-Tol-BZ was obtained as a reddish-yellow solid [Scheme 1]. $^1$H-NMR (Fig. S1, δ): 4.65 and 4.78 (s, 4H, -N–$CH_2$–Ar), 5.39 and 5.41 (s, 4H, -O-$CH_2$ –N), 8.34 (s, 2H, –N=CH-). $^{13}$C-NMR (Fig. S1) δ: 50.54 (-N–$CH_2$–Ar), 80.50 (-O-$CH_2$–N), 145.50 (-N-Ar), 117–135 (phenyl carbons).

### 2.3. Polymerization of Schiff base functional BZ monomer (SF-Tol-BZ)

The thermosetting polybenzoxazine, known as poly(SF-Tol-BZ), was synthesized by subjecting around 0.001 g of SF-Tol-BZ monomer to a curing process in an oven. The curing process involved a step profile with temperatures of 120, 140, 160, 180, 200, and 210 °C, each for a duration of 2 h. As the temperature increased, the material's color gradually changed from reddish yellow to

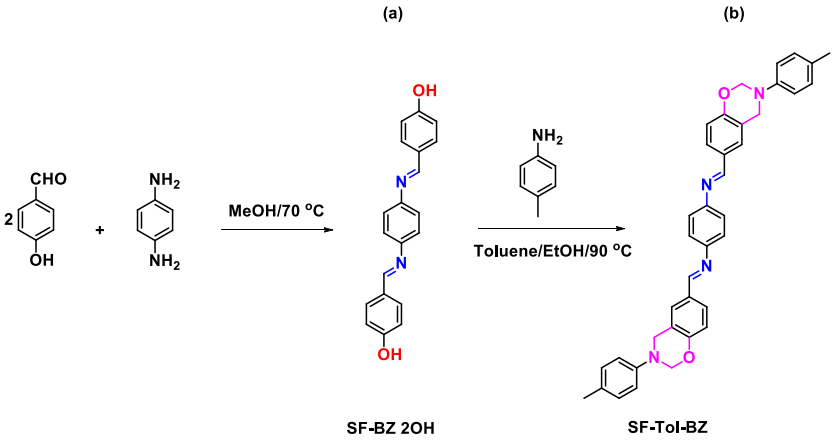


**Scheme 1.** Representing the synthesis of SF-Tol-BZ monomer.

black. The synthesis procedure and chemical structures of the SF-Tol-BZ monomer and its resulting poly(SF-Tol-BZ) are illustrated in Scheme 2.

### 2.4. Preparation of poly(SF-Tol-BZ) coatings on mild steel (MS)

The MS used in this study had a chemical composition of 0.19% Mn, 0.05% Si, 0.022% Cu, 0.94% C, 0.009% P, 0.004% S, 0.014% Ni, 0.009% Cr, 0.016% V, 0.003% Ti, 0.034% Al, and 98.709% Fe [9], and was obtained from the Egyptian Petroleum Research Institute. Before coating, the surface of the MS substrates (10 × 20 × 1 mm) was polished with sandpaper and then washed with acetone, methanol, and water. The substrates were then dried under a vacuum. A series of chloroform solutions containing different concentrations of SF-Tol-BZ (50, 100, 150, 200, and 300 g/L) was prepared, filtered through the paper to remove insoluble residues, and used to coat the MS substrates by a dip coating method. The film thickness of all samples was kept constant at approximately 2 μm. The coated MS samples were air-dried for 24 h and then cured in an oven at 200 °C for 2 h.

## 3. Results and discussion

### 3.1. Polymerization behavior of SF-Tol-BZ

The Schiff base functionalized benzoxazine was analyzed using DSC and FTIR techniques to study its polymerization behavior. The ring-opening polymerization (ROP) of BZ monomer is known to be influenced by synergistic hydrogen bonding interactions. Previous studies have shown that blending benzoxazine with chitosan leads to a remarkable reduction in the ROP temperature of benzoxazine to 70 °C, due to the formation of Schiff base structure [36]. In the present study, the SF-Tol-BZ monomer showed a low melting point of approximately 65 °C based on the DSC chart [Fig. 1], which may be attributed to the crystalline regions [37]. This low melting point suggests that the SF-Tol-BZ has good processing performance. The DSC thermograms for the uncured SF-Tol-BZ monomer after different curing processes are presented in Fig. 1. The exothermic peak (curing temperature) for the uncured SF-Tol-BZ was observed at around 253 °C. We observed that the exothermic peak gradually decreased after each thermal curing stage. The exothermic peak completely disappeared after curing at 180 °C, indicating complete ROP. The poly(SF-Tol-BZ) cured at 240 °C exhibited a high $T_g$ of 210 °C, as observed from the DSC thermogram. This value is significantly higher than that poly(DIS-PA-meaxfa100-x) [38]. To gain a deeper understanding of the ROP behavior of SF-Tol-BZ (Fig. 2), further investigation was carried out using FTIR. Following the curing process at 180 °C, the characteristic absorption bands at 1229 and 921 $cm^{-1}$, associated with the C–O–C and oxazine rings, respectively, were completely absent. This observation aligns with the findings from the DSC analysis, reinforcing the obtained results.

### 3.2. Thermogravimetric analysis (TGA) of SF-Tol-BZ

The delocalization of π electrons in polymers with long conjugated π bonds generally leads to higher thermal resistance, as reported in the literature [39,40]. To investigate the thermal stability of the SF-Tol-BZ and its polymers at different curing stages, TGA was performed. As depicted in Fig. 3, the onset of degradation and char yield of the samples increased with increasing curing temperature, due to the cross-linking in the thermosetting polymer via the ROP of the oxazine unit and liquid crystal (LC) structure [41]. The C=N imine linker and the π conjugated electrons resulted in the formation of excess cross-linking points in the system. The poly(SF-Tol-BZ) exhibited a char yield of 54 wt% under $N_2$ (at 800 °C), indicating excellent fire resistance [42]. Among the cured samples, the poly (SF-Tol-BZ) thermoset cured at 240 °C showed the highest thermal stability, with an onset of degradation (10 wt% loss) above 604 °C. This value is one-time higher than that reported for the LC polybenzoxazine in previous studies [43]. The higher onset of degradation temperature is due to the formation of the nematic phase structure at a temperature of approximately 120 °C, mainly due to the better ability of the mesogenic Schiff base to form LC, which also acts as a center cross-link of the PBZ network. These results

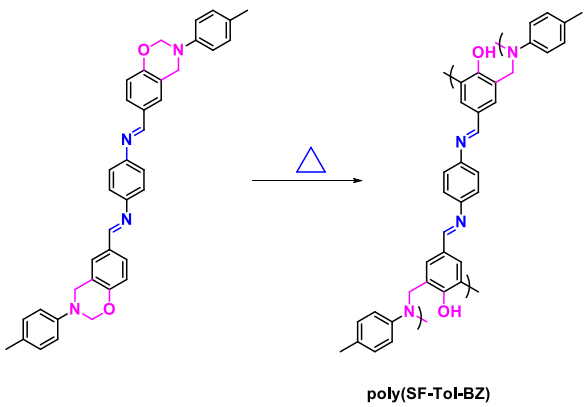


**Scheme 2.** Thermal curing polymerization to produce poly(SF-Tol-BZ) from SF-Tol-BZ precursor.

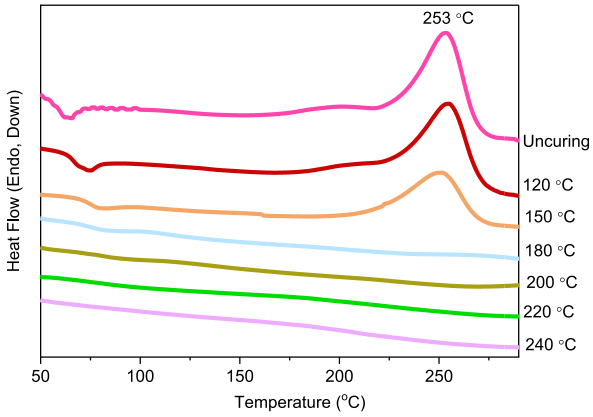


**Fig. 1.** DSC thermograms of uncuring SF-Tol-BZ monomer and after different curing process.

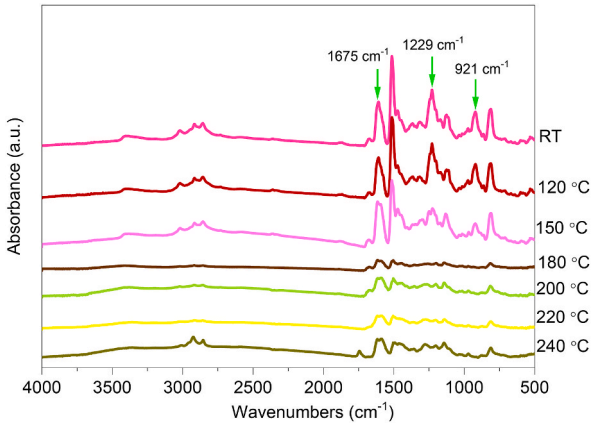


**Fig. 2.** FTIR spectra of uncuring SF-Tol-BZ monomer and after different curing process.

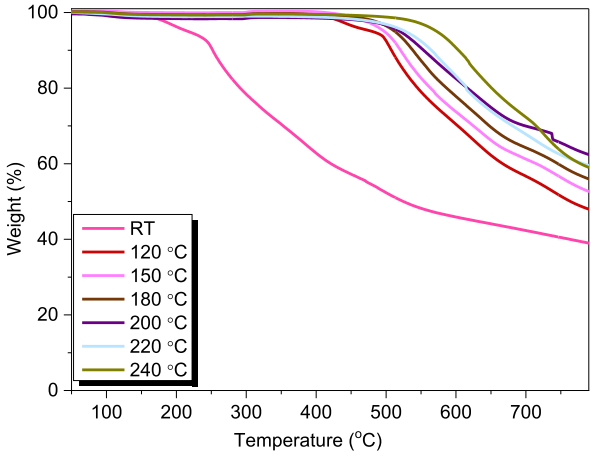


**Fig. 3.** TGA of uncuring SF-Tol-BZ monomer and after different curing process.

suggest that the Schiff base-based BZ is a promising material for high-temperature applications with a wide processing temperature range for subsequent thermal recycling processes. A summary of the thermal properties of The poly(SF-Tol-BZ) at different curing stages is presented in Table 1. The poly(SF-Tol-BZ) precursors demonstrated a $CO_2$ uptake of 23 mg $g^{-1}$ (at 298 K, Fig. S2).

### 3.3. Corrosion evaluations of poly(SF-Tol-BZ) coatings

The corrosion resistance of poly(SF-Tol-BZ) coatings on MS was evaluated using electrochemical impedance spectroscopy (EIS), open circuit potential (OCP), and potentiodynamic polarization. OCP-time measurements of the coating were conducted at different concentrations of the polymer and bare MS, as illustrated in Fig. 4. The values of OCP of the coating samples in a 3.5% aqueous solution of NaCl varied compared to bare MS. However, as the concentration of the polymer increased, a more positive shift in OCP values was observed, indicating that poly(SF-Tol-BZ) coatings have a high ability to prevent the corrosion of MS. The maximum shift in OCP values was −250 mV for the polymer coating at a concentration of 300 g/L, which is about one order of magnitude higher than that reported for quinazoline Schiff base inhibitors [16]. This first result under OCP conditions suggests that the poly(SF-Tol-BZ) coatings can disrupt or inhibit redox reactions on the surface of MS [44]. The positive shift in OCP values with increasing concentrations of polymer coatings indicates the toughness of the layer surface for polymer coatings, thus the optimal corrosion protection [45].

### 3.4. Potentiodynamic polarization measurements

We also conducted a potentiodynamic polarization test on both bare and coated MS samples to obtain the Tafel plot. The experiment was carried out in a 3.5% aqueous solution of NaCl with different concentrations of poly(SF-Tol-BZ) at room temperature, with a scan speed of 0.4 mV/s from −1000 to −100 mV, as shown in Fig. 5. By extrapolating the cathodic and anodic Tafel lines, they determined the corrosion current density ($I_{corr}$) and corrosion potential ($E_{corr}$). They also calculated the percentage of corrosion protection efficiencies (IE %) using the following formula (1) [46].

$$IE\ \% = \frac{I_{corr} - I_{corr(c)}}{I_{corr}} \times 100 \tag{1}$$

where $I_{corr}$ is the corrosion current obtained for bare MS and $I_{corr}$(c) is the corrosion current for coated MS. Also, the corrosion rate(CR) values were calculated using the following formula (2) [47,48]:

$$CR = \frac{I_{corr} \times K \times EW}{\rho A} \tag{2}$$

Where K is the corrosion rate constant (3272 mm year$^{-1}$), EW is the equivalent weight for MS (27.9 g), ρ the density of MS (7.85 g cm$^{-3}$), and A is the sample area (1 cm$^2$).

The results of the potentiodynamic polarization and Tafel plot analyses are summarized in Table 2 and Fig. 5. The data show that the poly(SF-Tol-BZ) coatings have a significant effect on both the anodic and cathodic Tafel slopes, especially at concentrations of 200 and 300 g/L. As the concentration of the polymer coating increased, both the anodic and cathodic reactions were gradually suppressed. The corrosion protection efficiency of the coatings was also improved by shifting the $E_{corr}$ values to more positive potentials. For example, the $E_{corr}$ values shifted from −946 mV for bare MS to −721 mV for coated MS at a concentration of 50 g/L, and to −319 mV for coated MS at 150 g/L. A more electropositive value indicates the formation of a passive layer on the MS surface. As the concentration of the coating increased to 200 and 300 g/L, the $E_{corr}$ values shifted to negative potentials of −432 and −503 mV, respectively, indicating that the coating can be used as a mixed inhibitor [49]. The $I_{corr}$ and CR values of the coatings also significantly decreased as the concentration of Schiff base based PBZ increased. The coating at a concentration of 300 g/L exhibited the best protective behavior against corrosion, with the lowest value of $I_{corr}$ [50,51]. The maximum protection efficiency of 92.26% was achieved at 300 g/L for the poly(SF-Tol-BZ). Poly(SF-Tol-BZ) coatings exhibit exceptional corrosion protection due to the incorporation of key functional groups such as –C=N-, phenolic groups (-OH), and aromatic rings. These structural elements are responsible for the superior anti-corrosive properties observed in the MS when coated with poly(SF-Tol-BZ) [16]. Overall, the results demonstrate that poly(SF-Tol-BZ) coatings have a high ability to prevent corrosion of MS, and the corrosion protection efficiency of the coatings is significantly improved with increasing concentration.

### 3.5. EIS measurements

EIS is a valuable tool for studying corrosion as it provides essential insights into the properties of a metal surface, electrochemical kinetics, and coating adsorption by analyzing impedance spectra [52]. In this study, the corrosion behavior of MS in a 3.5% NaCl

**Table 1**
TGA results of SF-Tol-BZ before and after thermal treatments.

| Sample code | Cure temp (°C) | $T_{d5}$ (°C) | $T_{d10}$ (°C) | Char yield at 800 °C |
|---|---|---|---|---|
| **SF-Tol-BZ** | RT | 216 | 252 | 39 |
| | 120 | 480 | 508 | 41 |
| | 150 | 497 | 521 | 42 |
| | 180 | 512 | 538 | 48 |
| | 200 | 520 | 554 | 54 |
| | 220 | 548 | 586 | 53 |
| | 240 | 572 | 604 | 51 |

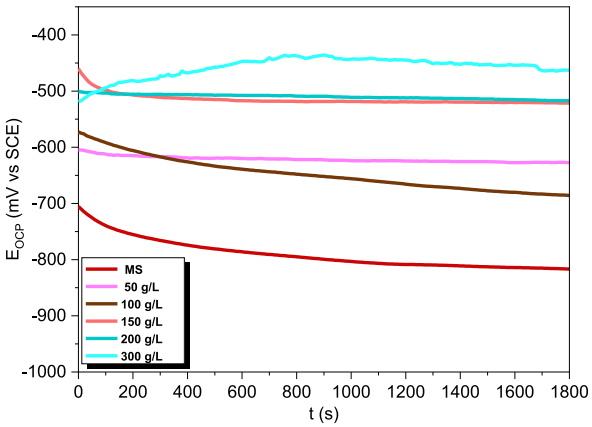


**Fig. 4.** OCP-time plots of bare MS and poly(SF-Tol-BZ) coatings at different concentrations.

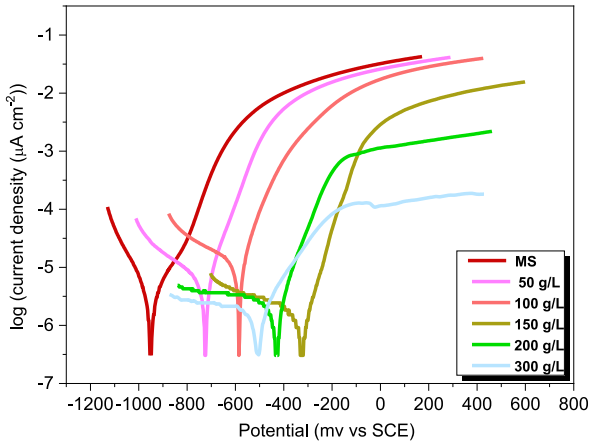


**Fig. 5.** Tafel plots of bare MS and poly(SF-Tol-BZ) coatings at different concentrations.

**Table 2**
Tafel results of Schiff base based PBZ coatings at different concentrations.

| Samples | $E_{corr}$ (mv) | $I_{corr}$ (μA cm$^{-2}$) | $R_P$ (KΩ) | CR (μm year$^{-1}$) | IE (%) | Surface coverage (θ) |
|---|---|---|---|---|---|---|
| MS | −951 | 15.5 ± 0.6 | 2.4 ± 0.2 | 98 ± 0.6 | – | – |
| 50 g/L | −726 | 4.1 ± 0.4 | 2.8 ± 0.4 | 51 ± 0.4 | 73.55 ± 0.2 | 0.74 |
| 100 g/L | −584 | 3.5 ± 0.2 | 2.9 ± 0.5 | 48 ± 0.5 | 77.42 ± 0.3 | 0.77 |
| 150 g/L | −325 | 3.0 ± 0.2 | 3.2 ± 0.3 | 32 ± 0.3 | 80.65 ± 0.4 | 0.81 |
| 200 g/L | −432 | 2.3 ± 0.3 | 6.2 ± 0.4 | 30 ± 0.2 | 89.19 ± 0.3 | 0.89 |
| 300 g/L | −503 | 1.2 ± 0.5 | 15.3 ± 0.8 | 22 ± 0.2 | 92.26 ± 0.6 | 0.92 |

solution was investigated using EIS at room temperature, both with and without poly(SF-Tol-BZ) coatings. Fig. 6 and S3 display the Nyquist plot of both the bare MS and coated MS at varying concentrations of poly(SF-Tol-BZ). The impedance Z was measured as a function of frequency ω, which consists of two components, real (Zr) and imaginary (Zi) impedance, resulting from the system's resistance and capacitance/inductance elements, respectively. The Nyquist plots for both MS and coated MS had the same shape but with increased diameters, indicating enhanced resistivity. At low frequencies, non-ideal semicircles were observed in the loops, revealing the non-ideal behavior of the double layers as a capacitor due to frequency dispersion resulting from the MS surface's non-homogeneity and roughness [9]. In order to accurately represent coatings with heterogeneities in their mesostructure and chemical composition, it was determined that utilizing the constant phase element (CPE) is more appropriate for describing the double-layer capacitance at the interface between the electrode and electrolyte, as opposed to relying solely on the ideal electrical capacitance [53]. The impedance of CPE is expressed using the following formula (3) [54].

$$Z_{CPE} = \frac{1}{Y_0(jw)^n} \tag{3}$$

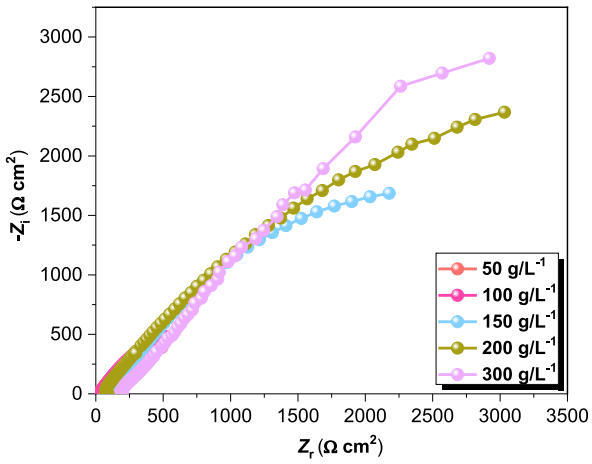


**Fig. 6.** Nyquist plots of poly(SF-Tol-BZ) coatings at different concentrations.

Where $Y_0$ is the magnitude of the CPE, j is an imaginary unit, ω is an angular frequency ($\omega = 2\pi f$), where f is the coating frequency and n is the phase shift. The results obtained from EIS analysis (presented in Table 3) indicate that an increase in the concentration of Schiff base-based PBZ results in an increase in charge transfer resistance ($R_{ct}$) and a decrease in double-layer capacitance $C_{dl}$ (CPE), indicating reduced porosity of the coatings and improved protection against corrosive agents. These EIS results are consistent with Tafel and Eocp-time results, where the sample coating with a concentration of 300 g/L showed the highest corrosion protection performance. When compared to bare MS, $R_{ct}$ increased by 9 times and $C_{dl}$ decreased by one order of magnitude for the sample coating with a concentration of 200 g/L. However, when the concentration of the polymer coating was increased to 300 g/L, $R_{ct}$ increased by 24 times. Fig. 7 presents the Bode plots of MS and coated MS at different concentrations of poly(SF-Tol-BZ). In the low-frequency range, it was observed that the Z modules of the coated MS at the concentration of 300 g/L increased by around four orders of magnitude more than those of bare MS, indicating an improved barrier property of the poly(SF-Tol-BZ) coating on MS. At a frequency of 0.01 Hz, the mild steel coated with a concentration of 300 g/L of the newly introduced coating demonstrates the highest |Z| value. This value is considerably greater than that observed for the previously reported PBza-d400 coating by Zhao et al [55].

### 3.6. Corrosion protection mechanism

The key mechanism responsible for the corrosion prevention capability of MS involves the adsorption of coating molecules onto its surface, as depicted in Fig. 8. This adsorption process can occur either chemically or physically, leading to the formation of a protective layer. The adsorption process is influenced by various factors, including the functional group, electron density of donor atoms, and the interaction between the p and d orbitals of the coating and the MS surface. Previous research indicates that when Schiff base is adsorbed on MS surfaces in 1 M HCl solutions, chemisorption tends to dominate over physisorption [13]. The adsorption process is mainly driven by the exchange reaction between the coating and $H_2O$ molecules, which can be expressed by the following equation (4):

$$Schif\ base\ PBZ_{sol} + \times(H_2O)_{ads} \rightarrow Schif\ base\ PBZ_{ads} + H_2O_{sol} \quad (4)$$

Where $Schif\ base\ PBZ_{ads}$ is the coating that adsorbed on the MS surface in the salt solution, and X is the number of $H_2O$ molecules that are displaced by the Schiff base-based PBZ coating. Additionally, the coating molecules combine with the newly produced $Fe^{2+}$ ions, resulting MS-coating complex as shown in the following Equations (5) and (6):

$$Fe \rightarrow Fe^{+2} + 2e^{-} \quad (5)$$

$$Fe^{+2} + Schif\ base\ PBZ_{ads} \rightarrow [Fe - Schif\ base\ PBZ]^{+2}_{(ads)} \quad (6)$$

Where $[Fe - Schif\ base\ PBZ]^{+2}_{(ads)}$ presents the $Fe^{+2}$-coating complex at the interface

### 3.7. Scanning electron microscopy (SEM)

Fig. 9 presents the results of SEM analysis conducted on both bare and coated mild steel (MS) substrates before and after electrochemical testing. In Fig. 9(a), the surface of the bare MS substrate appears rough, indicating a well-polished surface. However, after exposure to a corrosive medium (3.5% NaCl solution), Fig. 9(b) reveals a high concentration of corrosion products on the surface of the bare MS substrate. In contrast, Fig. 9(c) displays the SEM image of the poly(SF-Tol-BZ) coating on MS after the corrosion tests. It shows a smooth and fully covered surface, devoid of any pits or cracks. This observation is similar to the surface morphology of the PBza-d400-coated steel reported previously [55]. The findings indicate that the application of poly(SF-Tol-BZ) coatings effectively

**Table 3**
EIS results of Schiff base based PBZ coatings at different concentrations.

| Samples | $R_s$ ($\Omega$ $cm^2$) | CPE(F) | n | $R_{ct}$ ($\Omega$ $cm^2$) | References |
|---|---|---|---|---|---|
| MS | 18.6 | $6.64 \times 10^{-4}$ | 0.824 | 1340 | This work |
| 50 g/L | 21.1 | $3.31 \times 10^{-4}$ | 0.711 | 1970 | This work |
| 100 g/L | 30 | $3.06 \times 10^{-4}$ | 0.710 | 4840 | This work |
| 150 g/L | 47.9 | $6.73 \times 10^{-5}$ | 0.718 | 5570 | This work |
| 200 g/L | 81.9 | $5.59 \times 10^{-5}$ | 0.653 | 9370 | This work |
| 300 g/L | 120.3 | $3.21 \times 10^{-5}$ | 0.655 | 24230 | This work |
| MMDQ at concentration of 1.0 mM | 0.88 | – | 0.84 | 245.157 | [13] |
| PBA–AN(0.5 mg mL) | – | – | 0.83 | 23200 | [34] |

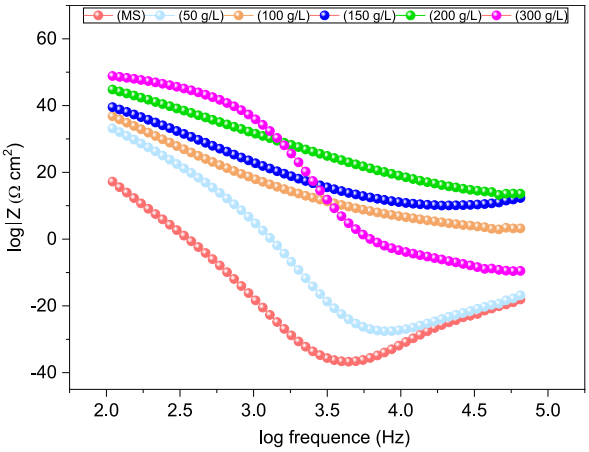


**Fig. 7.** Bode plots of bare MS and poly(SF-Tol-BZ) coatings at different concentrations.

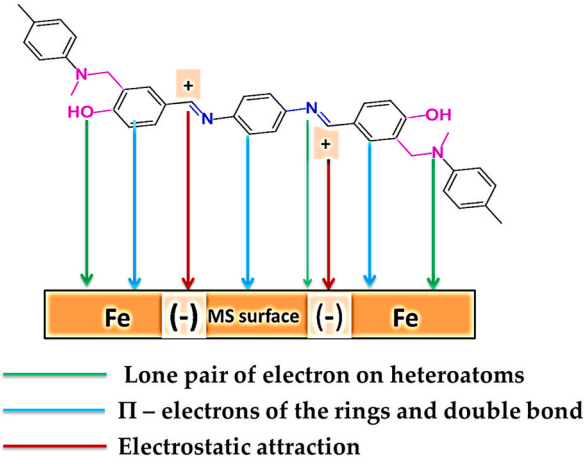


**Fig. 8.** Corrosion protection mechanism of poly(SF-Tol-BZ) coating on MS.

mitigates the rapid dissolution of MS by facilitating the adhesion of coating molecules to its surface. This adhesion process creates a protective barrier that significantly reduces the rate of corrosion of MS in a 3.5% NaCl solution.

## 4. Conclusions

In this study, the molecular design of benzoxazine was successfully achieved by incorporating a Schiff base moiety into the benzoxazine. The resulting BZ, named SF-Tol-BZ, exhibited complete ROP at a lower temperature of 180 °C, compared to traditional benzoxazines like SA-Hex-BZ, which required 210 °C for complete ROP. This improved reactivity was attributed to the presence of the catalyst Schiff base moiety in SF-Tol-BZ. Furthermore, thermalgravimetric analysis (TGA) results demonstrated that poly(SF-Tol-BZ)

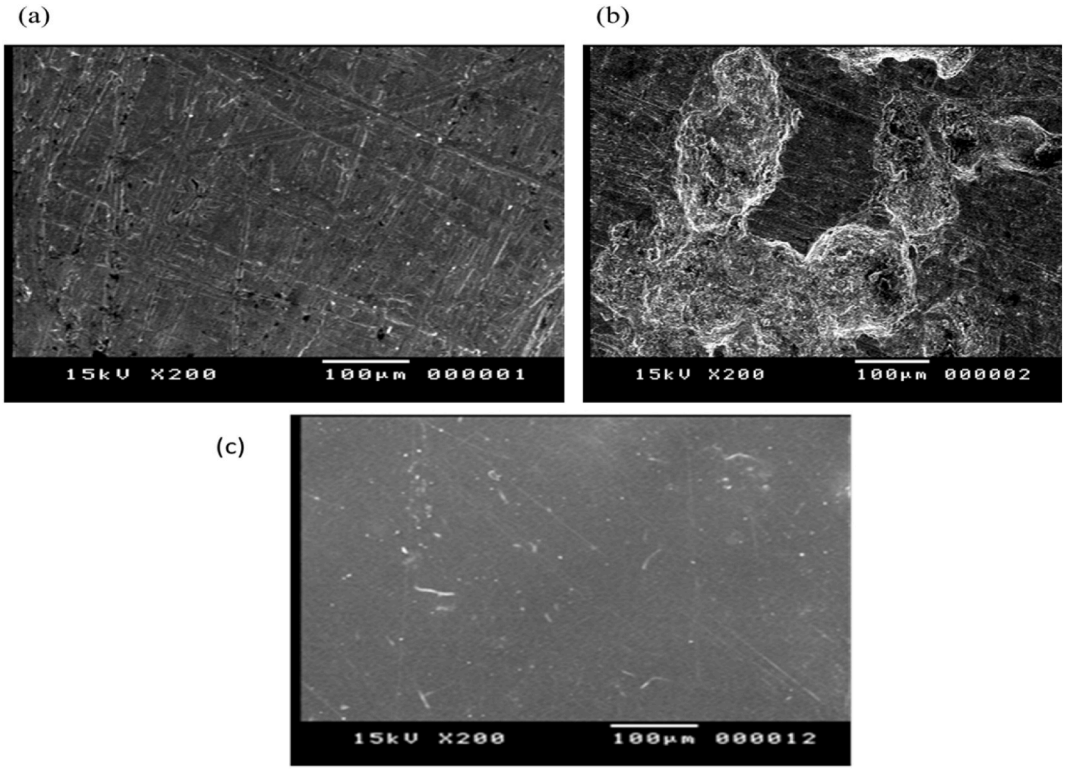


**Fig. 9.** SEM images of MS before (a) and after immersion in 0.5% NaCl without (b) and with (c) 300 g/L of SF-Tol-BZ, for 0.5 h at 35 °C.

cured at 240 °C exhibited excellent thermal stability, maintaining stability up to 604 °C. This suggests that the material holds promise for high-temperature applications. Poly(SF-Tol-BZ) coatings were prepared on MS at various concentrations and subjected to thermal curing. These coatings displayed high efficiency in protecting MS against corrosion in a 3.5% NaCl solution. At a concentration of 300 g/L, the coatings achieved a corrosion protection efficiency of 92.3%, with an associated corrosion current density ($I_{corr}$) of 1.2 μA/cm$^2$. Notably, the $I_{corr}$ value of poly(SF-Tol-BZ) was more than two orders of magnitude lower than that of poly(SA-Hex-BZ) (243 μA/cm$^2$). The enhanced corrosion protection observed in the poly(SF-Tol-BZ) coatings can be attributed to the presence of specific functional groups such as –C=N-, phenolic (-OH) groups, and aromatic rings. These functional groups play a crucial role in promoting better adsorption of the polymer onto the mild steel (MS) surface. As a result, they contribute to the improved corrosion resistance offered by the coating. This finding was corroborated by SEM surface morphology analysis. Moreover, the decrease in double-layer capacitance values, represented by CPE) with increasing polymer coating concentration indicates the formation of a thicker electrical double-layer and a lower local dielectric constant. These factors contribute to the effective corrosion protection of the coating by facilitating its adsorption at the metal/solution interface.

## Author contribution statement

Abdulsalam Mahdy: Conceived and designed the experiments; Performed the experiments. Kamal I. Aly: Contributed reagents, materials, analysis tools or data. Mohamed Gamal Mohamed: Conceived and designed the experiments; Analyzed and interpreted the data; Wrote the paper.

## Data availability statement

The data that has been used is confidential.

## Declaration of competing interest

The authors declare that they have no known competing financial interests or personal relationships that could have appeared to influence the work reported in this paper.

## Appendix A. Supplementary data

Supplementary data to this article can be found online at https://doi.org/10.1016/j.heliyon.2023.e17977.

## References


[1] A.A. Al-Amiery, W.N.R.W. Isahak, W.K. Al-Azzawi, Corrosion inhibitors: natural and synthetic organic inhibitors, Lubricants 11 (2023) 174, https://doi.org/10.3390/lubricants11040174.

[2] E.B. Caldona, C. Al-Christopher, B.B. Pajarito, R.C. Advincula, Novel anti-corrosion coatings from rubber-modified polybenzoxazine-based polyaniline composites, Appl. Surf. Sci. 422 (2017) 162–171, https://doi.org/10.1016/j.apsusc.2017.05.083.

[3] A. Elaine, M. Alvaro, C.A. Ferreira, C. Aleman, Polyaniline, polypyrrole and poly(3,4-ethylenedioxythiophene) as additives of organic coatings to prevent corrosion, Surf. Coating. Technol. 203 (2009) 3763–3769, https://doi.org/10.1016/j.surfcoat.2009.06.019.

[4] A. Alamiery, Corrosion inhibition effect of 2-N-phenylamino-5-(3-phenyl-3-oxo-1-propyl)-1, 3, 4-oxadiazole on mild steel in 1 M hydrochloric acid medium: insight from gravimetric and DFT investigations, Mater. Sci. Technol. 4 (2021) 398–406, https://doi.org/10.1016/j.mset.2021.09.002.

[5] M.G. Mohamed, S.W. Kuo, A. Mahdy, I.M. Ghayd, K.I. Aly, Bisbenzylidene cyclopentanone and cyclohexanone-functionalized polybenzoxazine nanocomposites: synthesis, characterization, and use for corrosion protection on mild steel, Mater. Today Commun. 25 (2020), 101418, https://doi.org/10.1016/j.mtcomm.2020.101418.

[6] M.G. Mohamed, A. Mahdy, R.J. Obaid, M.A. Hegazy, S.-W. Kuo, K.I. Aly, Synthesis and characterization of polybenzoxazine/clay hybrid nanocomposites for UV light shielding and anti-corrosion coatings on mild steel, J. Polym. Res. 28 (2021) 297, https://doi.org/10.1007/s10965-021-02657-0.

[7] A.A. Alamiery, Anticorrosion effect of thiosemicarbazide derivative on mild steel in 1 M hydrochloric acid and 0.5 M sulfuric Acid: gravimetrical and theoretical studies, Mater. Sci. Technol. 4 (2021) 263–273, https://doi.org/10.1016/j.mset.2021.07.004.

[8] M. Chakravarthy, K. Mohana, C.P. Kumar, Corrosion inhibition effect and adsorption behaviour of nicotinamide derivatives on mild steel in hydrochloric acid solution, Int. J. Ind. Chem. 5 (2014) 1–21, https://doi.org/10.1007/s40090-014-0019-3.

[9] K.I. Aly, A. Mahdy, M.A. Hegazy, N.S. Al-Muaikel, S.W. Kuo, M.G. Mohamed, Corrosion resistance of mild steel coated with phthalimide-functionalized polybenzoxazines, Coating 10 (2020) 1114, https://doi.org/10.3390/coatings10111114.

[10] P.S. Gaikwad, A.S. Krieg, P.P. Deshpande, S.U. Patil, J.A. King, M. Maiaru, G.M. Odegard, Understanding the origin of the low cure shrinkage of polybenzoxazine resin by computational simulation, ACS Appl. Polym. Mater. 3 (2021) 6407–6415, https://doi.org/10.1021/acsapm.1c01164.

[11] M.G. Mohamed, W.-C. Chang, S.-W. Kuo, Crown ether-and benzoxazine-linked porous organic polymers displaying enhanced metal ion and $CO_2$ capture through solid-state chemical transformation, Macromolecules 55 (2022) 7879–7892, https://doi.org/10.1021/acs.macromol.2c01216.

[12] M.G. Mohamed, M.M. Samy, T.H. Mansoure, C.J. Li, W.C. Li, J.H. Chen, S.W. Kuo, Microporous carbon and carbon/metal composite materials derived from bio-benzoxazine-linked precursor for $CO_2$ capture and energy storage applications, Int. J. Mol. Sci. 23 (2022) 347, https://doi.org/10.3390/ijms23010347.

[13] M.G. Mohamed, C.J. Li, M.A.R. Khan, C.C. Liaw, K. Zhang, S.W. Kuo, Formaldehyde-free synthesis of fully bio-based multifunctional bisbenzoxazine resins from natural renewable starting materials, Macromolecules 55 (2022) 3106–3115, https://doi.org/10.1021/acs.macromol.2c00417.

[14] M.G. Mohamed, T.-C. Chen, S.-W. Kuo, Solid-state chemical transformations to enhance gas capture in benzoxazine-linked conjugated microporous polymers, Macromolecules 54 (2021) 5866–5877, https://doi.org/10.1021/acs.macromol.1c00736.

[15] M.G. Mohamed, S.-W. Kuo, Crown ether-functionalized polybenzoxazine for metal ion adsorption, Macromolecules 53 (2020) 2420–2429, https://doi.org/10.1021/acs.macromol.9b02519.

[16] G. Khan, W.J. Basirun, S.N. Kazi, P. Ahmed, L. Magaji, S.M. Ahmed, A.B.B.M. Badry, Electrochemical investigation on the corrosion inhibition of mild steel by Quinazoline Schiff base compounds in hydrochloric acid solution, Colloid Interface Sci. 502 (2017) 134–145, https://doi.org/10.1016/j.jcis.2017.04.061.

[17] H.A. Sorkhabi, B. Shabani, B. Aligholipour, D. Seifzadeh, The effect of some Schiff bases on the corrosion of aluminum in hydrochloric acid solution, Appl. Surf. Sci. 252 (2006) 4039–4047, https://doi.org/10.1016/j.apsusc.2005.02.148.

[18] M. Ehteshamzade, T. Shahrabi, M. Hosseini, Inhibition of copper corrosion by self-assembled films of new Schiff bases and their modification with alkanethiols in aqueous medium, Appl. Surf. Sci. 252 (2006) 2949–2959, https://doi.org/10.1016/j.apsusc.2005.05.003.

[19] J. Talati, M. Desai, N. Shah, Meta-substituted aniline-N-salicylidenes as corrosion inhibitors of zinc in sulphuric acid, Mater. Chem. Phys. 93 (2005) 54–64, https://doi.org/10.1016/j.matchemphys.2005.02.004.

[20] M. Behpour, S.M. Ghoreishi, N. Mohammadi, M.S. Niasari, Investigation of the inhibiting effect of N-[(Z)-1-phenylemethyleidene]-N-{2-[(2-{[(Z)-1phenylmethylidene] amino} phenyl) disulfanyl] phenyl} amine and its derivatives on the corrosion of stainless steel 304 in acid media, Corros. sci. 53 (2011) 3380–3387, https://doi.org/10.1016/j.corsci.2011.06.017.

[21] H.A. Sorkhabi, B. Shaabani, D. Seifzadeh, Corrosion inhibition of mild steel by some Schiff base compounds in hydrochloric acid, Appl. Surf. Sci. 239 (2005) 154–164, https://doi.org/10.1016/j.apsusc.2004.05.143.

[22] M.N. Desai, M.B. Desai, C.B. Shah, S.M. Desai, Schiff bases as corrosion inhibitors for mild steel in hydrochloric acid solutions, Corros. sci. 26 (1986) 827–837, https://doi.org/10.1016/0010-938X(86)90066-1.

[23] N.L. Chen, P.P. Kong, H.X. Feng, Y.Y. Wang, D.Z. Bai, Corrosion mitigation of chitosan Schiff base for Q235 steel in 1.0 M HCl, J. Bio- Tribo-Corros. 5 (2019) 1–8, https://doi.org/10.1007/s40735-019-0219-7.

[24] M. Ramanathan, G. Rajendran, S. Sethumanickam, Eco-friendly chitosan vanillin Schiff base as anti-corrosive agent for mild steel in 1 M HCl and as scale inhibitor for $CaCO_3$, J. Adhes. Sci. Technol. 36 (2022) 1–24, https://doi.org/10.1080/01694243.2022.2066401.

[25] G. Lu, J. Dai, J. Liu, S. Tian, Y. Xu, N. Teng, X. Liu, A new sight into bio-based polybenzoxazine: from tunable thermal and mechanical properties to excellent marine antifouling performance, ACS Omega 5 (2020) 3763–3773, https://doi.org/10.1021/acsomega.0c00025.

[26] K.I. Aly, A.A. Amer, M.H. Mahross, M.R. Belal, A.M. Soliman, M.G. Mohamed, Construction of novel polybenzoxazine coating precursor exhibiting excellent anti-corrosion performance through monomer design, Heliyon 9 (2023), e15976, https://doi.org/10.1016/j.heliyon.2023.e15976.

[27] T.S. Haubold, A. Hartwig, K. Koschek, Synthesis and application studies of DOPO-based organophosphorous derivatives to modify the thermal behavior of polybenzoxazine, Polymers 14 (2022) 606, https://doi.org/10.3390/polym14030606.

[28] M.M. Iqbal, S. Appasamy, B. Krishnasamy, H. Arumugam, R.V. Maheshwari, B. Vigneshwaran, A. Muthukaruppan, Development of sustainable polybenzoxazine-based organic–inorganic hybrid nanocomposites for high voltage insulator applications, J. Mater. Sci. Mater. Electron. 34 (2023) 603, https://doi.org/10.1007/s10854-022-09805-2.

[29] I. Tiwari, P. Sharma, L. Nebhani, Polybenzoxazine-an enticing precursor for engineering heteroatom-doped porous carbon materials with applications beyond energy, environment and catalysis, Mater. Today Chem. 23 (2022), 100734, https://doi.org/10.1016/j.mtchem.2021.100734.

[30] S. Zachariah, Y.L. Liu, Nanocomposites of polybenzoxazine-functionalized multiwalled carbon nanotubes and polybenzoxazine for anticorrosion application, Compos. Sci. Technol. 194 (2020), 108169, https://doi.org/10.1016/j.compscitech.2020.108169.

[31] E.B. Caldona, A.C.C. De Leon, P.G. Thomas, D.F. Naylor III, B.B. Pajarito, R.C. Advincula, Superhydrophobic rubber-modified polybenzoxazine/$SiO_2$ nanocomposite coating with anticorrosion, anti-ice, and superoleophilicity properties, Ind. Eng. 56 (2017) 1485–1497, https://doi.org/10.1021/acs.iecr.6b04382.

[32] C.Y. Chen, W.C. Chen, M.G. Mohamed, Z.Y. Chen, S.W. Kuo, Highly thermally stable, reversible, and flexible main chain type benzoxazine hybrid incorporating both polydimethylsiloxane and double-decker shaped polyhedral silsesquioxane units through diels–alder reaction, Macromol. Rapid Commun. 44 (2023), 2200910, https://doi.org/10.1002/marc.202200910.

[33] W. Zhang, N. Jiang, T. Zhang, T. Zhang, Preparation and properties of silane-modified cardanol–benzoxazine for hydrophobic coating, J. Elastomers Plast. 53 (2021) 296–310, https://doi.org/10.1177/0095244320933988.
[34] Z. Jamain, N.F. Omar, M. Khairuddean, Synthesis and determination of thermotropic liquid crystalline behavior of cinnamaldehyde-based molecules with two Schiff base linking units, Molecules 25 (2020) 3780, https://doi.org/10.3390/molecules25173780.
[35] A. Mahdy, M.G. Mohamed, K.I. Aly, H.B. Ahmed, H.E. Emam, Liquid crystalline polybenzoxazines for manufacturing of technical textiles: water repellency and ultraviolet shielding, Polym. Test. 119 (2023), 107933, https://doi.org/10.1016/j.polymertesting.2023.107933.
[36] M. Monisha, N. Yadav, B. Lochab, Sustainable framework of chitosan–benzoxazine with mutual benefits: low curing temperature and improved thermal and mechanical properties, ACS Sustain. Chem. Eng. 7 (2019) 4473–4485, https://doi.org/10.1021/acssuschemeng.8b06515.
[37] A. Van, K. Chiou, H. Ishida, Use of renewable resource vanillin for the preparation of benzoxazine resin and reactive monomeric surfactant containing oxazine ring, Polymer 55 (2014) 1443–1451, https://doi.org/10.1016/j.polymer.2014.01.041.
[38] A. Adjaoud, L. Puchot, P. Verge, High-tg and degradable isosorbide-based polybenzoxazine vitrimer, ACS Sustain. Chem. Eng. 10 (2021) 594–602, https://doi.org/10.1021/acssuschemeng.1c07093.
[39] İ. Kaya, F. Kolcu, G. Demiral, H. Ergül, E. Kiliç, Synthesis and characterization of imine polymers of aromatic aldehydes with 4-amino-2-methylquinoline via oxidative polycondensation, Des, Monomers Polym 18 (2015) 89–104, https://doi.org/10.1080/15685551.2014.971395.
[40] A. Mahdy, M. Al-azzany, Synthesis, characterization and thermal properties of photoresponsive epoxy resin containing benzylidene units in the main chain, Albaydha University J. 4 (2022), https://doi.org/10.56807/buj.v4i03.333.
[41] C. Farren, M. Akatsuka, Y. Takezawa, Y. Itoh, Thermal and mechanical properties of liquid crystalline epoxy resins as a function of mesogen concentration, Polymer 42 (2001) 1507–1514, https://doi.org/10.1016/S0032-3861(00)00499-7.
[42] I. Machado, E. Rachita, E. Fuller, V.M. Calado, H. Ishida, Very high-char-yielding elastomers based on the copolymers of a catechol/furfurylamine benzoxazine and polydimethylsiloxane oligomers, ACS Sustain. Chem. Eng. 9 (2021) 16637–16650, https://doi.org/10.1021/acssuschemeng.1c05408.
[43] Y. Liu, J. Chen, Y. Qi, S. Gao, K. Balaji, Y. Zhang, Z. Lu, Cross-linked liquid crystalline polybenzoxazines bearing cholesterol-based mesogen side groups, Polymer 145 (2018) 252–260, https://doi.org/10.1016/j.polymer.2018.05.004.
[44] A. Hermas, M. Morad, A comparative study on the corrosion behaviour of 304 austenitic stainless steel in sulfamic and sulfuric acid solutions, Corrosion Sci. 50 (2008) 710–2717, https://doi.org/10.1016/j.corsci.2008.06.029.
[45] F.S. de Souza, A. Spinelli, Caffeic acid as a green corrosion inhibitor for mild steel, Corros. sci. 51 (2009) 642–649, https://doi.org/10.1016/j.corsci.2008.12.013.
[46] V. Selvaraj, T. Raghavarshini, M. Alagar, Evaluation of thermo-mechanical, dielectric and corrosion resistant properties of cardanol benzoxazine-epoxy based hybrid composites: a very low temperature curing pre-polymer for high performance paint related applications, High Perform. Polym. 32 (2020) 524–539, https://doi.org/10.1177/0954008319885006.
[47] M.A. Hegazy, M. Abdallah, M. Alfakeer, H. Ahmed, Corrosion inhibition performance of a novel cationic surfactant for protection of carbon steel pipeline in acidic media, Int. J. Electrochem. Sci. 13 (2018) 6824–6842, https://doi.org/10.20964/2018.07.53.
[48] M. Hagarová, J. Brezinová, G. Baranová, J. Viňáš, P. Maruschak, Degradation of components in cars due to bimetallic corros, Mat 14 (2021) 3323, https://doi.org/10.3390/2Fma14123323.
[49] K.I. Aly, M.G. Mohamed, O. Younis, M.H. Mahross, M. Abdel-Hakim, M.M. Sayed, Salicylaldehyde azine-functionalized polybenzoxazine: synthesis, characterization, and its nanocomposites as coatings for inhibiting the mild steel corrosion, Prog. Org. Coating 138 (2020), 105385, https://doi.org/10.1016/j.porgcoat.2019.105385.
[50] T.A. Fabijanić, M. Kurtela, I. Škrinjarić, J. Pötschke, M. Mayer, Electrochemical corrosion resistance of Ni and Co bonded near-nano and nanostructured cemented carbides, Metals 10 (2020) 224, https://doi.org/10.3390/met10020224.
[51] F. Zulkifli, M.S.M. Yusof, M.I.N. Isa, A. Yabuki, W.W. Nik, Henna leaves extract as a corrosion inhibitor in acrylic resin coating, Prog. Org. Coating 105 (2017) 310–319, https://doi.org/10.1016/j.porgcoat.2017.01.017.
[52] S. Li, C. Zhao, H. Gou, H. Li, Y. Li, D. Xiang, Synthesis and characterization of aniline-dimer-based electroactive benzoxazine and its polymer, RSC Adv. 7 (2017) 55796–55806, https://doi.org/10.1039/C7RA11349H.
[53] C. Zhou, X. Lu, Z. Xin, J. Liu, Y. Zhang, Polybenzoxazine/$SiO_2$ nanocomposite coatings for corrosion protection of mild steel, Corrosion Sci. 80 (2014) 269–275, https://doi.org/10.1016/j.corsci.2013.11.042.
[54] M.A. Hegazy, R.M. Samy, A. Labena, M.A. Wadaan, W.N. Hozzein, 4, 4′-(((1E, 5E)-pentane-1, 5-diylidene) bis (azanylylidene)) bis (1-dodecylpyridin-1-ium) bromide as a novel corrosion inhibitor in an acidic solution (part I), Mater. Sci. Eng. C. 110 (2020), 110673, https://doi.org/10.1016/j.msec.2020.110673.
[55] C. Zhao, J. Wei, J. Wu, Y. Li, D. Xiang, Y. Wu, Z. Hou, Synthesis and characterization of polyetheramine-type benzoxazines as protective coatings for low carbon steel against corrosion in sodium chloride solution, Int. J. Electrochem. Sci. 17 (2022), https://doi.org/10.20964/2022.06.43.